Perturbing an electromagnetically induced transparency in a Λ system using a low-frequency driving field. I. Three-level system

E. A. Wilson, N. B. Manson, and C. Wei
Laser Physics Center, Research School of Physical Sciences and Engineering, Australian National University, Canberra, Australian Capital Territory, 0200, Australia

Yang Li-Jun
College of Physical Sciences and Technology, Hebei University, Baoding 071002, China
(Received 20 May 2005; published 23 December 2005)

Electromagnetically induced transparency (EIT) resonance in a Λ configuration is obtained when the frequencies of two fields are close to resonance with two of the transitions and their frequency difference matches the frequency of the third transition. In this situation the spectrum of one swept field as a probe gives a simple transparency feature. However, when an additional field drives the third transition the EIT feature associated with the probe is split. This perturbed EIT is illustrated for both single and bichromatic driving fields. In the single-driving-field case a density matrix treatment is shown to be in reasonable agreement with experiment, and in both single and bichromatic cases the structure in the spectrum can be explained using the dressed-state formalism. The dressed states can also be used to account for subharmonic resonances observed in the strong-probe regime.

DOI: 10.1103/PhysRevA.72.063813 PACS number(s): 42.50.Gy, 42.50.Nn, 76.30.Mi

I. INTRODUCTION

There has been considerable interest in the phenomenon of electromagnetically induced transparency (EIT) [1–3] because of applications associated with gain and lasing without inversion [4], enhanced susceptibilities [5], ultraslow light [6], and light storage [7]. The applications are based on the ability of one light field to strongly modify the spectral properties of the medium for a second light field. In the simplest case there are two fields and three levels and this situation has been studied extensively and covered by review articles [8]. Recently there has been interest in controlling the EIT by using an additional electromagnetic field, and in this work this is discussed in terms of the EIT being perturbed by the extra field. We have considered previously one case where an extra "light" field is introduced and couples the levels involved in the EIT to a fourth level [9]. There are similar studies for gases [10]. In the present work the perturbation is restricted to the three-level system. There are three levels and three fields and we are not aware of studies where EIT has been perturbed in this way.

The situation to be discussed is an EIT in a three-level Λ system with inhomogeneous broadening in the high-frequency transitions but near-homogeneous broadening in the low-frequency transition. That is, there are two lower hyperfine levels $|1\rangle$ and $|2\rangle$ and the energy separation between the levels is taken to have a fixed value. There is one upper level $|3\rangle$ (Fig. 1) but there is a distribution in its energy with respect to levels $|1\rangle$ and $|2\rangle$. The coupling field is applied near resonance with the $|2\rangle$-$|3\rangle$ transition and a conventional EIT is observed when probing transition $|1\rangle$-$|3\rangle$. The EIT is perturbed by driving the transition between the two lower levels, $|1\rangle$-$|2\rangle$. Experimental measurement of such a situation has been reported for spin levels in a color center in diamond [11,12]. Splittings were observed but no detailed calculation was presented [12] and one of the motivations for this paper is to correct this situation. The situation is modeled and modest comparison made with the experimental traces obtained using a density matrix formalism. In addition the observations are explained in terms of the dressed states of the driven system and this dressed-state approach is extended to account for experimental measurements also presented in this paper. The measurements involve perturbing an EIT with a bichromatic field and also observation of resonances obtained when using strong coupling and probe fields.

The EIT spectra reported are for radio frequency fields, but the phenomena are general and analogous effects are possible at visible wavelengths. At radio frequencies sources are readily available, the optical and rf double-resonance techniques give very efficient detection of the rf responses, and these factors combined with the unusual properties of the diamond color center provide an avenue for studying EIT and related effects. The authors take advantage of the conditions to study the effect an additional field has on an EIT.

II. EXPERIMENT

The experiments involve measurements of spin transitions within the ground state of the nitrogen-vacancy center in diamond. The ground state is an orbital singlet and the electron spin has $S=1$ and nuclear spin $I=1$ and the absorption of the spin transitions are determined using rf and optical techniques. An account of the color center and experimental techniques has been given in previous publications [9,13,14] and only an outline is given here. The detection involves Raman heterodyne detection, which is a wave mixing scheme where it is possible to detect the signal associated with one rf response in the presence of other rf fields. The experiments involve a $2\times2\times2$ mm^3 diamond cube with a

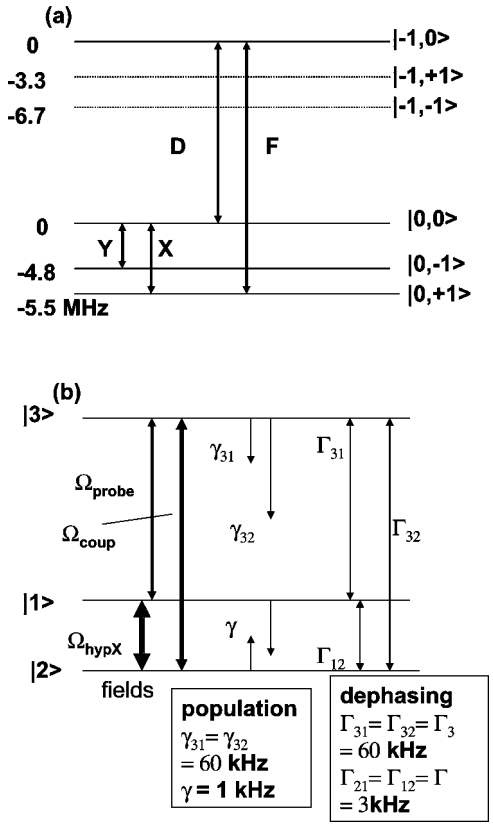

FIG. 1. (a) Energy levels of the ground state of the nitrogen-vacancy color center in diamond used in the experiments. The ground state is an orbital singlet with $S=1$ and $I=1$ and a magnetic field is used to bring the spin levels $|M_s=-1\rangle$ and $|M_s=0\rangle$ close to an avoided crossing. In this situation the three upper hyperfine levels $|M_s=-1,M_I=\pm1,0\rangle$ are typically 40 MHz higher in energy than the lower hyperfine levels ($|M_s=0,M_I=\pm1,0\rangle$ for a magnetic field of 1000 G. The relative energies of the states are given and the arrows indicate the transitions involved in the study. (b) Energy levels, fields, and decay rates used in experiments and theoretical treatment. The three levels are the same as those given in (a) and designated by the simpler notation $|1\rangle$, $|2\rangle$, and $|3\rangle$. The experiments involve the application of three fields simultaneously. The coupling field and probe field have Rabi frequencies of Ω_{coup} and Ω_{probe}, respectively. The perturbation field is applied resonant with the X transition with Rabi frequency Ω_{hypX}.

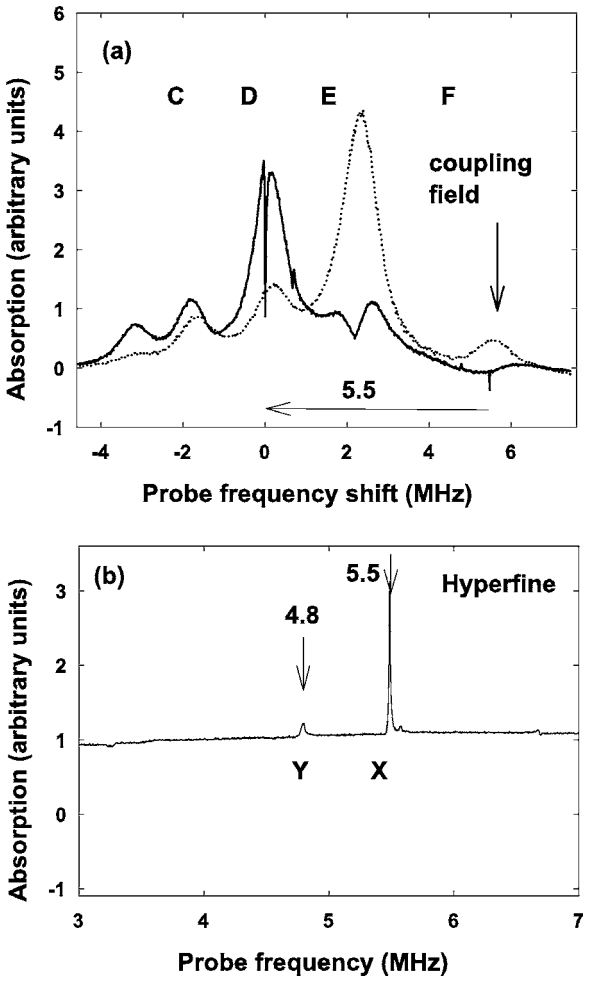

FIG. 2. (a) Electron spin resonance spectrum of nitrogen-vacancy center in diamond measured using the Raman heterodyne technique. The measurements are made about a central frequency of 40 MHz corresponding to a situation close to an anticrossing of spin levels. C, D, and E are the three allowed lines associated with the nuclear spin of the nitrogen, $M_I=+1$, 0, and -1, and the other lines are induced in first order of the magnetic field misalignment with the trigonal axis of the center. The dashed trace gives the spectrum obtained for a weak probe in the absence of other fields whereas the solid line gives the spectrum when a strong coupling ($\Omega_F=60$ kHz) field is applied resonant with the transition F. A transparency is induced in the D transition at a frequency shift of 5.5 MHz from the frequency of the coupling field. The separation corresponds to the frequency of the hyperfine transition X (see Fig. 1). (b) Spectrum of hyperfine transitions measured using the Raman heterodyne technique.

nitrogen-vacancy concentration of 10^{18} cm^{-3} cooled to helium temperatures. The transmission of a 20 mW laser beam resonant with the optical transition at 637 nm is detected with a fast pin diode and with the Raman heterodyne technique the out-of-phase modulation at the frequency of the probe rf field gives a measure of the absorption of the electron spin transition. The probe field and other driving rf fields are applied to a six-turn coil wound round the crystal. The unusual aspect of Raman heterodyne scheme for this color center is that the laser also pumps the population into a single electron spin level $|M_s=0\rangle$ and this leads to greatly enhance detection sensitivity. Raman heterodyne requires optical transitions to be allowed to a common excited state and is achieved by working close to an avoided crossing with a magnetic field of 1030 G along a crystallographic $\langle 111\rangle$ direction. Six spin levels are involved in the crossing and three of these are used in the present studies; one hyperfine level of the upper electron spin state and two hyperfine levels of the lower spin state [Fig. 1(a)]. The inhomogeneous width of the electron spin transition has a width of 1 MHz as can be seen from Fig. 2(a) whereas the homogeneous width and population relaxation can be determined from separated Raman heterodyne electron spin-echo and spin-recovery measurements. Both are found to have values of the order of 60 kHz [9]. From Fig. 2(b) the hyperfine transitions have a linewidth of the order of 3 kHz and echo measurements

show that these linewidths are only slightly increased from the homogeneous width of 1 kHz. In the calculations the hyperfine transition is assumed to be homogeneous with a width of 3 kHz. (This assumption of a homogenous broadened hyperfine transition gives some limitations to the calculations as will be discussed.) For the subset of centers used, the relaxation within the hyperfine levels is similar to that of the homogeneous linewidth of the order of 1 kHz. The energies and transitions are summarized in Fig. 1(a). We probe an allowed transition D corresponding to the $|M_s=0,M_I=0\rangle$-$|M_s=-1,M_I=0\rangle$) transition, and the coupling field is applied resonant with the F transition ($|M_s=0,M_I=+1\rangle$-$|M_s=-1,M_I=0\rangle$). For brevity the $|M_s,M_I\rangle$ states $|0,0\rangle$, $|0,+1\rangle$, and $|-1,0\rangle$ are denoted $|1\rangle$, $|2\rangle$, and $|3\rangle$, respectively. These states and the driving fields are summarized in Fig. 1(b) together with population and coherence relaxation rates used in the calculations. We choose the $|2\rangle$ level as the lowest as it leads to formulation similar to other EIT publications [1,3].

In the absence of a perturbing field a sharp EIT transparency is observed within the D transition and this spectrum is shown in Fig. 2(a) whereas Fig. 2(b) shows a direct measure of the hyperfine transitions. We study how the EIT feature in Fig. 2(a) is changed by the application of a perturbing field resonant with a ground-state hyperfine transition X. In an associated study we also consider the effect of applying a perturbing field Y resonant with a second hyperfine transition and this will be presented in a separate paper [15].

III. DENSITY MATRIX CALCULATION

The N-V system used in this study is a multilevel system. There are nine ground-state spin levels and 18 optical excited-state levels. An optical field resonant with the ground- to excited-state transition is used for detection but it is weak and there is negligible population in the optical levels. The light field pumps population into the $|M_s=0\rangle$ electron spin state and with the external magnetic field there is also some preferential population of the nuclear hyperfine levels. Most of the population is in the $|M_s=0,M_I=+1\rangle$, $|1\rangle$ state, with less in the $|M_s=0,M_I=0\rangle$, $|2\rangle$ state and less still in the $|M_s=0,M_I=-1\rangle$ state. This means that the majority of the population is in states $|1\rangle$ and $|2\rangle$. The driving field couples these levels to the excited $|M_s=-1,M_I=0\rangle$, $|3\rangle$ level. Little of the population leaves the three levels $|1\rangle$, $|2\rangle$, and $|3\rangle$ and it can be modeled as a closed three-level system. The relaxation between the levels can be modeled using an equilibrium population value for each of the three levels or with an effective relaxation between the levels, and the latter approach is used in the following calculations.

The coupling field is resonant with the $|2\rangle$-$|3\rangle$ transition and the $|1\rangle$-$|3\rangle$ transition is probed, giving the standard EIT for the Λ situation. The EIT feature occurs where the frequency difference of the probe and coupling field matches the frequency of the $|1\rangle$-$|2\rangle$ transition. The perturbing field is introduced resonant with this transition and a theoretical treatment of the situation is described in this section. The population differences are defined as $W_{21}=\rho_{22}-\rho_{11}$ and $W_{31}=\rho_{33}-\rho_{11}$ and the density matrix equations can then be written as

$$\begin{aligned}
\dot{W}_{21} &= -2\gamma W_{21} - i\chi_{probe}(\rho_{31}e^{i\delta t} - \rho_{13}e^{-i\delta t}) + i\chi_{coup}(\rho_{32} - \rho_{23}) \\
&\quad - 2i\chi_{hypX}(\rho_{21} - \rho_{12}), \\
\dot{W}_{31} &= -\gamma_3/2 - (\gamma - \gamma_3/2)W_{21} - \gamma_3 W_{31} \\
&\quad - 2i\chi_{probe}(\rho_{31}e^{i\delta t} - \rho_{13}e^{-i\delta t}) - i\chi_{coup}(\rho_{32} - \rho_{23}) \\
&\quad - i\chi_{hypX}(\rho_{21} - \rho_{12}), \\
\dot{\rho}_{31} &= d_{31}\rho_{31} - i\chi_{probe}e^{-i\delta t}W_{31} + i\chi_{coup}\rho_{21} - i\chi_{hypX}\rho_{32}, \\
\dot{\rho}_{21} &= d_{21}\rho_{21} - i\chi_{hypX}W_{21} - i\chi_{probe}\rho_{23}e^{-i\delta t} + i\chi_{coup}\rho_{31}, \\
\dot{\rho}_{32} &= d_{32}\rho_{32} + i\chi_{probe}\rho_{12}e^{-i\delta t} - i\chi_{coup}(W_{31} - W_{21}) - i\chi_{hypX}\rho_{31}.
\end{aligned} \tag{1}$$

The population decays γ and γ_3 have been defined in Fig. 1(b). The complex detunings d_{ij} are defined as

$$\begin{aligned}
d_{31} &= i\delta_{31} - \Gamma_{31}, \\
d_{32} &= i\delta_{32} - \Gamma_{32}, \\
d_{21} &= i\delta_{21} - \Gamma_{21},
\end{aligned} \tag{2}$$

where Γ_{ij} are the dephasing rates of the transition between levels i and j and the detunings δ_{ij} are defined as

$$\begin{aligned}
\delta_{32} &= \omega_{coup} - \omega_{32}, \quad \delta_{21} = \omega_{hypX} - \omega_{21}, \\
\delta_{31} &= \omega_{coup} + \omega_{hypX} - \omega_{31} = \delta_{32} + \delta_{21}, \\
\delta &= \omega_{probe} - \omega_{coup} - \omega_{hypX}.
\end{aligned} \tag{3}$$

It is convenient to write the Rabi frequencies as $\Omega_{probe}=2\chi_{probe}$, $\Omega_{coup}=2\chi_{coup}$, and $\Omega_{hypX}=2\chi_{hypX}$ for the probe, coupling, and hyperfine perturbing fields, respectively. To calculate the absorption profile of the transition $|1\rangle$-$|3\rangle$ using a weak field of frequency ω_{probe}, we obtain a steady-state solution for ρ_{31}. The solution is derived perturbatively to the first order of the probe Rabi frequency Ω_{probe} using the Floquet expansion method [16]. Details are given in the Appendix. The absorption profile of the probe is obtained by plotting the imaginary part of the first-order solutions of the off-diagonal density matrix element $\rho_{31}^{(1)}$ as a function of probe detuning $\delta_{31}=\omega_{probe}-\omega_{31}$.

As we are dealing with a three-level "atom" interacting with three fields in a cyclic configuration there is a special case when the sum frequency of two fields exactly matches that of the third field. In this case the instantaneous response will be phase dependent and has been treated by other workers [17]. However, here the solutions correspond to the response of the probe field averaged over all phases. The coupling field and the hyperfine field are of fixed frequency and the swept probe field will only coincide with the frequency difference when within the detection bandwidth. The bandwidth can be 10 Hz, much smaller than the linewidth of the spectral features, 3 kHz. A single sweep can give a spike for the resonance situation but has different phases for each sub-

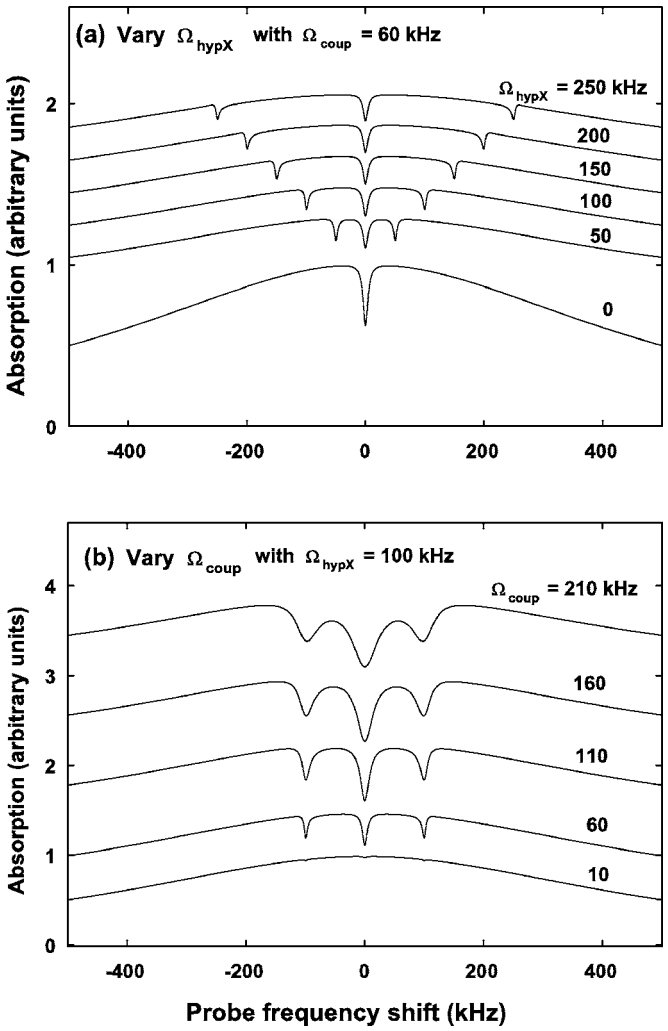

FIG. 3. Calculation of EIT for a homogeneously broadened three-level Λ system perturbed by a field applied resonant with the lowest transition. The traces (displaced for clarity) give the spectrum obtained by the solution of the density matrix equations given in the text. The calculations are those for a homogeneously broadened line with $\Gamma_{31}=\Gamma_{32}=1$ MHz. All other parameters are those for the experimental system as given in Fig. 1. (a) gives the spectrum for fixed coupling field strength and five different Rabi frequencies Ω_{hypX} of the perturbing field. (b) gives the equivalent for a fixed perturbing field and varying coupling field strength as indicated.

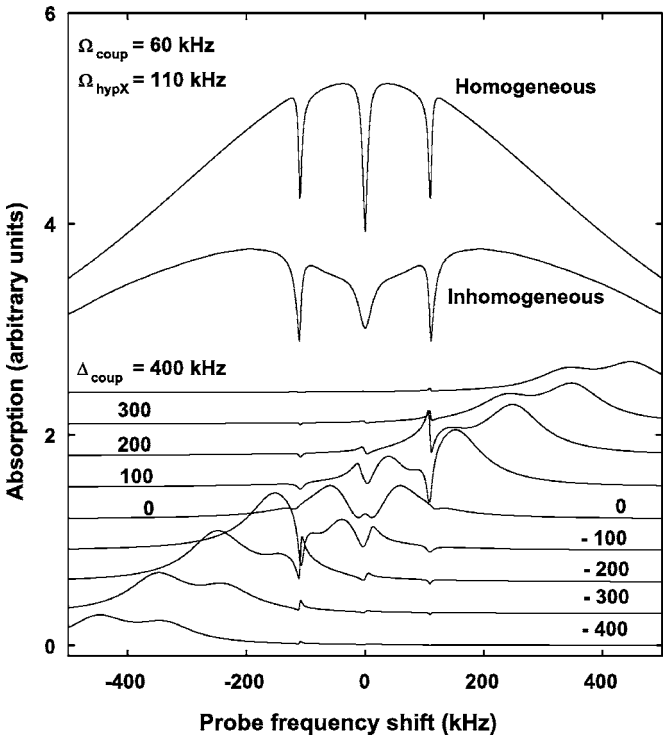

FIG. 4. Calculation of EIT for an inhomogeneously broadened three-level Λ system with perturbing field with Rabi frequency of $\Omega_{hypX}=110$ kHz applied resonant with the lowest transition. The lower traces show the spectrum for various homogeneous lines contributing to the inhomogeneous line. For these the resonant frequency is shifted and, hence, the coupling field is detuned from the individual resonance as indicated. A Gaussian distribution is assumed and the contribution summed to give the second top trace. The strengths of coupling field and perturbing field are indicated and the decay parameters are given in Fig. 1. The top trace is included for comparison. It gives the splitting for a homogeneous linewidth of 1 MHz with all other parameters the same as for the inhomogeneous case.

sequent sweep and averages to zero. Thus, it is straightforward to avoid the resonance response in the experimental traces.

The solutions for a homogeneously broadened system are illustrated in Fig. 3. We adopt a homogeneous width of 1 MHz whereas the other parameters are given their experimental values. The calculation gives a 60% deep transparency in the 1 MHz line for a coupling field with a Rabi frequency of 60 kHz [Fig. 3(a)]. With low coupling field strengths the EIT linewidth approximates the value assumed for the homogeneously broadened hyperfine transition of 3 kHz. Here the strength of coupling field causes some broadening and the EIT widths are of order of 8 kHz. A perturbing field with a Rabi frequency of Ω_{hypX} is applied resonant with the $|1\rangle$-$|2\rangle$ transition and this causes the EIT to be split into three transparencies with separations of Ω_{hypX}. Driving a transition with a resonant field does not cause broadening and, hence, in this case the driving field splits but does not add to the width of the features and so the three EIT features have similar widths to the undriven EIT case. This is illustrated in Fig. 3(a) for Rabi frequencies from $\Omega_{hypX}=50-250$ kHz. Compared with the parent EIT feature the transparencies are reduced in depth, with the unshifted EIT being deeper than the two satellite lines, but all are of similar widths. With a strong coupling field the central line is 100% and the satellite EIT's 50% and this situation is shown in Fig. 3(b). Further increase of the strength of the coupling field broadens each of the EIT features in a similar fashion to the situation where strong coupling fields broaden conventional EIT features.

The inhomogeneous broadening of the electron spin transitions can be modeled by repeating the above calculation for a frequency distribution of homogeneous lines and summing the individual contributions. Such a calculation is illustrated in Fig. 4 for the case of 1 MHz inhomogeneous and 60 kHz homogeneous linewidths. The lower traces indicate the con-

tribution of individual centers and these are summed to give the second top trace. The top trace shows the result of a calculation for a homogeneously broadened system. Had there been no hyperfine driving field the inclusion of inhomogeneous broadening would give rise to a modest increase in the parent EIT width, in the present case from 8 to 10 kHz. With the driving field present, including inhomogeneous broadening can be seen to give rise to a more significant increase in the transparency linewidths, which is larger for the central feature than for the satellites. There is the occurrence of a broad central spectral hole in the inhomogeneous spectrum due to a reduction in the contribution from near-resonant centers. The latter effect is dependent on the branching ratio of the population decay from the upper level $|3\rangle$ and the spectrum corresponds to that for equal decay to the two lower levels $|1\rangle$ and $|2\rangle$. The calculation has not taken into account any inhomogeneous broadening in the hyperfine transition.

IV. EXPERIMENTAL RESULTS AND COMPARISON WITH DENSITY MATRIX CALCULATION

The experimental measurements of EIT perturbed by an addition field in the three-level, three-field situation are shown in Fig. 5(a). A coupling field is applied resonant with the inhomogeneously broadened F transition and the D transition is probed [see Fig. 2(a)]. The on-resonant Rabi frequencies are Ω_{coup}=60 kHz driving the F transition and Ω_{probe}=0.5 kHz for the probed D transition. The relaxation parameters of the system have been given previously [9] and the Rabi frequencies of the applied fields are established from independent measurements. Therefore, all the relevant parameters are known and a solution of the above density matrix equations can be obtained by following the procedures given in the previous section. The result of the calculation is shown in the lower trace in Fig. 5(b) and can be compared with the experimental trace in Fig. 5(a). Equivalent experiments and calculations for various coupling field strengths are shown in Fig. 6. It is clear from these traces that the characteristics, such as the three-line pattern and broad hole, are in agreement but other details are not reliably predicted. In particular, there is a noticeably poor agreement in the width of the central EIT between experiment and calculation. No substantially better agreement has been obtained with minor variation of parameters used in the present calculation. Some of the inadequacy can be attributed to the inhomogeneous broadening of the hyperfine transition, which is not included in the current theoretical treatment. The hyperfine transition has a homogeneous width of 1 kHz and there is an inhomogeneous broadening of 3 kHz (whereas calculations have assumed a homogeneous broadening of 3 kHz). When driving such a transition near resonance with a Rabi frequency much higher than the linewidth, the positions of the features become determined by the frequency of the driving field plus or minus the Rabi frequency. Thus the small shifts in transition frequencies associated with inhomogeneous broadening are effectively quenched. The result is that the linewidth of features of a driven two-level system will approach the homogeneous linewidth and these are the linewidths to be expected in the present EIT case. By not including the 1–3 kHz broadening in our calculation, this narrowing will not occur and this can partially account for the disagreement between experiment and calculation. In future work a complete analysis including inhomogeneous broadening in both the electron spin and hyperfine transitions will be undertaken to investigate whether a more satisfactory agreement can be attained.

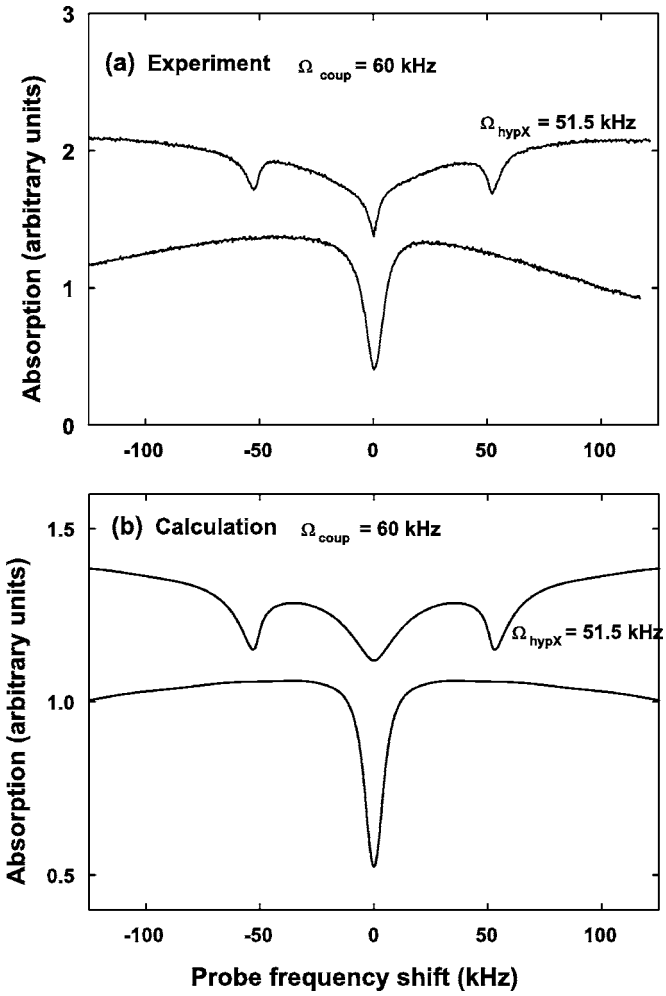

FIG. 5. (a) Experimental measurement of an EIT and that perturbed by a hyperfine driving field using spin levels in the nitrogen-vacancy center in diamond. Signals are obtained by the Raman heterodyne technique and give the absorption response of a weak (Ω_{probe}=0.5 kHz) rf source swept in frequency. The coupling field with a Rabi frequency of Ω_{coup}=60 kHz is applied resonant with the peak of the inhomogeneously broadened F transition and this gives rise to the EIT near the peak of the probed D transition, 5.5 MHz lower in frequency, as shown in the lower trace. The upper trace is obtained when a perturbing field with a Rabi frequency of Ω_{hypX}=51.5 kHz is applied resonant with the X transition. (b) Calculation of EIT and EIT with hyperfine perturbing field equivalent to experimental situation given in (a). The density matrix formulation is given in the text and these are solved for system decay parameters given in Fig. 1 and field strengths indicated.

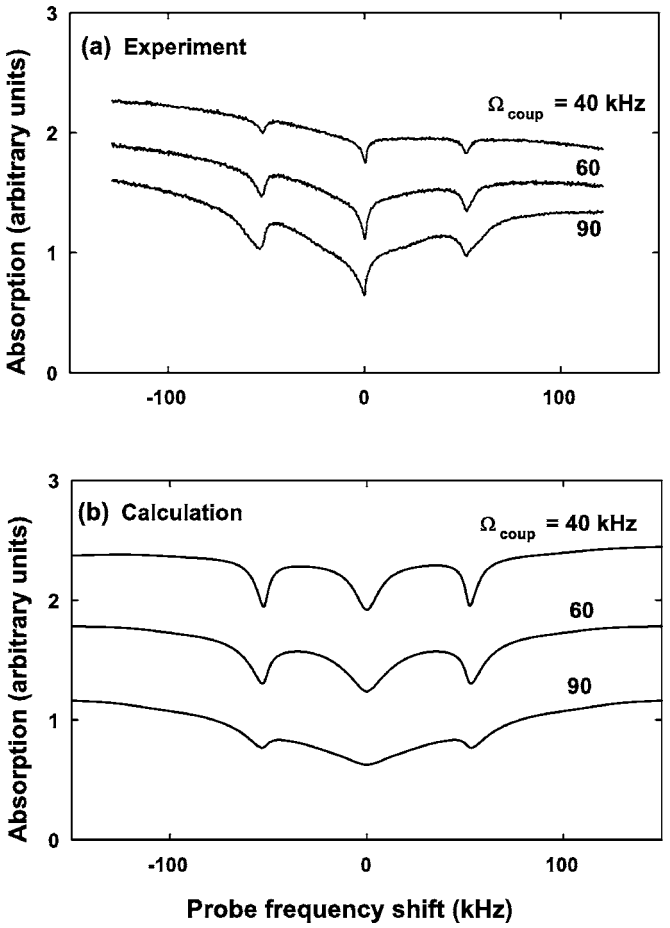

FIG. 6. (a) Experimental measurements of EIT perturbed by fixed hyperfine driving field with Ω_{hypX}=51.5 kHz but for three different strengths of coupling field as indicated. (b) Calculation of EIT as for Fig. 4(b) and field strengths equivalent to (a).

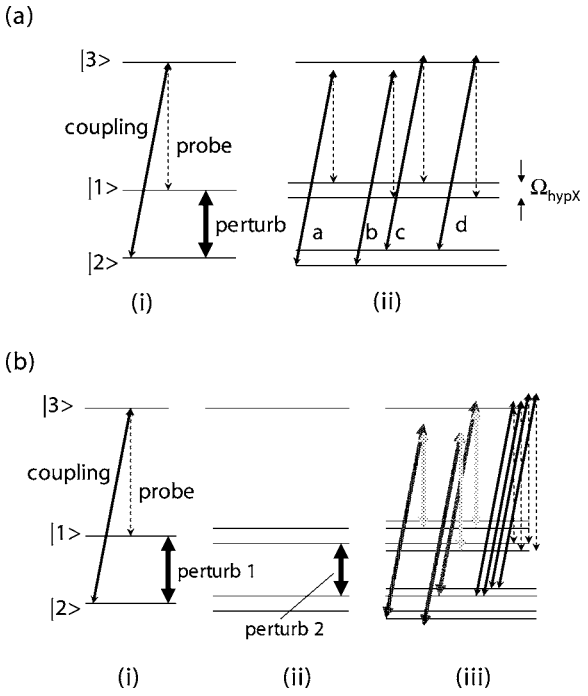

FIG. 7. Energy levels and dressed energy levels for EIT perturbed by (a) single and (b) bichromatic perturbing fields. (i) gives the bare states and fields. (ii) and (iii) give the dressed and doubly dressed states, respectively. In the dressed-state diagrams the coupling field is indicated by solid arrows and has the same frequency in each case. The probe is indicated by the dashed line and gives resonances at various frequencies as indicated. The splittings of the singly-dressed-state levels are associated with the first perturbing field and the smaller splitting of the doubly-dressed-state levels with the second perturbing field. In (iii) for brevity the transitions are only shown for the lowest-energy group of transitions.

V. DRESSED-STATE ANALYSIS

The positions of the spectral features are reliably predicted by the density matrix calculation. They can also be anticipated using the dressed states [18] of the hyperfine field shown in Fig. 7. It can be considered that the probed transition ($|2\rangle$-$|3\rangle$) is split into two with a separation of Ω_{hypX}. These two probe transitions are both inhomogeneously broadened to 1 MHz and so will overlap with each other. The coupling field gives rise to two EIT features (likewise separated by Ω_{hypX}) in each of the probed lines. When considering the overlapping transitions one pair of EIT features (b) and (c) coincide at zero frequency. The other EIT features, one within each probe transition, are displaced Ω_{hypX}. Thus, the predicted overall spectrum indicates a deeper central EIT [from (b) and (c)] and two weaker satellite EIT features [(a) and (d)] consistent with the experimental traces in Figs. 5 and 6.

The EIT feature occurs when the probe frequency in this case matches the frequency difference between the coupling and hyperfine transition frequencies $\omega_{probe}=\omega_{coupling}-\omega_{12}$. If there is a distribution of width δ_{12} in the frequency of the $|1\rangle$-$|2\rangle$ transition there will be a similar distribution in EIT frequencies. However, when the transition is driven the effective width of the EIT will be reduced to $\sqrt{(\delta_{12}^2+\Omega_{hypX}^2)}-\Omega_{12}$. Therefore, where there is inhomogeneous broadening of the hyperfine transitions the dressed-state model can also be used to account for the driving field causing a reduction in the distribution of EIT frequencies and a narrowing of all EIT features.

VI. BICHROMATIC PERTURBING FIELD

In this section we study the effect of applying a second perturbing field to the hyperfine transition $|1\rangle$-$|2\rangle$. We restrict the study to a special case where the second perturbing field is detuned in frequency by the Rabi frequency of the first perturbing field, Ω_{hypX}. This gives a resonant situation as the frequency of the second perturbing field coincides with a dressed-state transition (see Ref. [19]). Each of the single-field dressed-state levels is split in two, giving the doubly-dressed-state levels (Fig. 7). From analogous consideration to that given in the previous section it can be seen that the result is that each of the three EIT features obtained with a single driving field will itself be split into three.

The experimental measurements for such a bichromatic hyperfine perturbing field are shown in Fig. 8. The first hyperfine field is applied near resonant with the hyperfine tran-

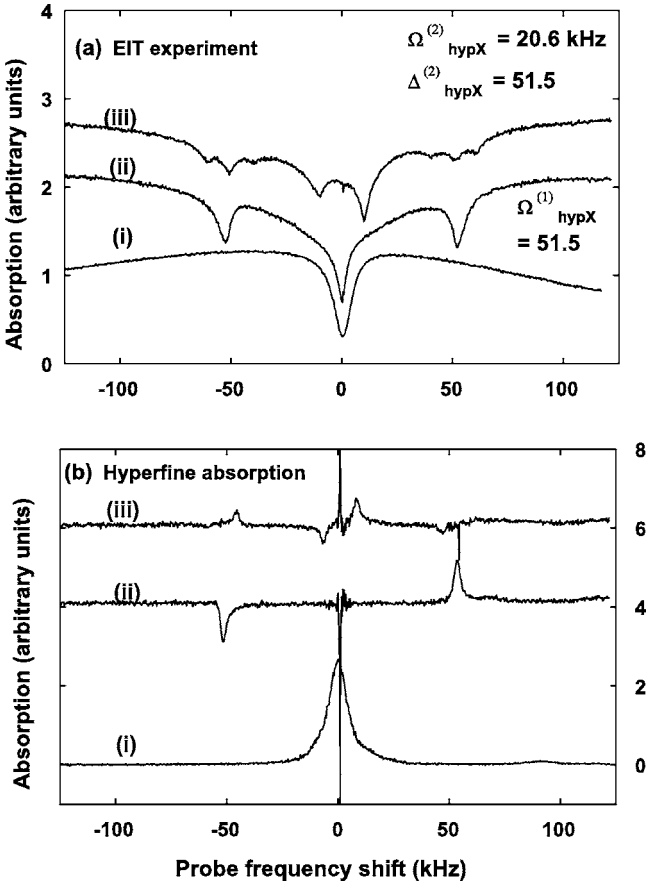

FIG. 8. (a) Experimental measurements of (i) EIT, (ii) EIT perturbed by single hyperfine driving field with Rabi frequency of Ω_{hypX}=51.5 kHz resonant with transition *X*, and (iii) EIT perturbed by a bichromatic field; the first component of the bichromatic field is equivalent to (ii) whereas the second is detuned by 51.5 kHz and has a Rabi frequency of Ω^2_{hypX}=20.6 kHz. (b) Raman heterodyne measurements of a weak probe field measuring the *X* hyperfine transition. The driving fields for traces (i), (ii), and (iii) are the same as those used in (a).

sition. The response is shown for a Rabi frequency of Ω_{hypX}=51.5 kHz and gives the three-line EIT spectrum as in the previous section. The second driving field has Rabi frequency of 20.6 kHz and is detuned by 51.5 kHz. The resultant spectrum is shown in the upper trace in Fig. 8(a). All three of the EIT features are split into three with separations of 10 kHz. The splittings are not well resolved but clearly the patterns are not the same for the three cases. The two satellite EIT features are each split in three with the central component stronger than the outer two. However, this is not the case for the central EIT feature where the magnitude of the splitting is the same but the middle component is weak or missing. A schematic of the dressed-state levels and transitions involved is shown in Fig. 7(b). The origin of the splitting is shown for the lower-energy features in detail but not duplicated for central and high-energy features. However, using this diagram the relative positions of the nine lines are readily justified as at 0, $\pm\Omega^{(2)}_{hypX}/2$, $\pm\Omega_{hypX}$, and $\pm\Omega_{hypX}\pm\Omega^{(2)}_{hypX}/2$. A much more elaborate treatment would be required to determine the magnitude of the transparencies using a dressed-state model but such a calculation has not been attempted.

VII. COMPARISON OF EIT WITH DIRECT PROBE OF HYPERFINE LEVELS

From the preceding section it can be seen that the two-photon EIT resonance provides a probe of the dressed states of the driven ground state. Clearly there will be a relationship between this spectrum and that obtained using a conventional one-photon weak-field probe. An experimental illustration of this comparison is presented in Fig. 8. Figure 8(a) has been described in the previous section and Fig. 8(b) gives the response of the driven system probing the hyperfine absorption directly. The one-photon probe of a driven two-level system is termed the Mollow spectrum [20,21] and has been reported by many groups. The one-photon probe of the bichromatic driven two-level system has also been reported previously [19]. The two-photon (EIT) probe shown here has not been reported previously to our knowledge. The relative positions of the features in the spectra are the same for the one- and two-photon probes but clearly the spectra have different characteristics. For example, with one photon the driving field equalizes population in the two-level system and significantly reduces the absorption response of a weak probe. Thus, the absorptions involving perturbing fields in Fig. 8(b) are significantly weaker than the parent absorption. This is not the case with the EIT spectrum. There are reductions in the equivalent EIT spectrum but not so marked as for a one-photon probe. Another way in which the spectra differ is in that the Mollow spectrum is very sensitive to the precise frequency [20]. The sign of the response depends on the frequency of the driving field and for the example used in Fig. 8(b) absorptive and emissive responses are observed. There is no such effect in the case of the EIT as all features are simple transparencies.

It is also worth noting the changes of linewidth of the features in the driven and un-driven systems. It has been mentioned before in Sec. IV that in a driven inhomogeneously broadened system the features can be narrowed when the Rabi frequency is larger than the inhomogeneous linewidth. This affect is clearly illustrated here in comparing traces (i) and (ii) in Fig. 8(b) where the driven system is probed directly. There is similar narrowing in the EIT spectrum, traces (i) and (ii) in Fig. 8(a), where the driven system is effectively probed via the two-photon process.

VIII. STRONG-PROBE EFFECTS

In the previous section it has been shown that there is relationship between one-photon and two-photon probes of a driven two-level system. It is known that the spectrum of a driven two-level system exhibits new resonances when the strength of the probe is increased. These resonances give features at integral fractions of the Rabi frequency of the driving field and are termed subharmonic resonances [14,22,23]. In this section it is shown that equivalent resonances can be observed in the two-photon (EIT) probe spectrum.

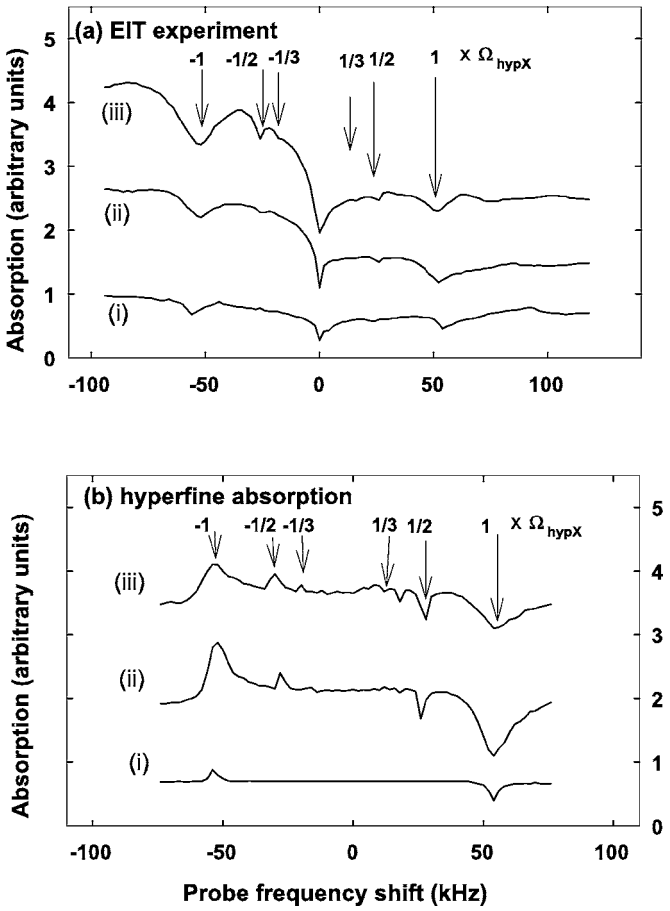

FIG. 9. (a) Experimental measurement of a perturbed EIT measured using strong probe fields. The perturbing field has a Rabi frequency of Ω_{hypX}=51.5 kHz and is resonant with transition *X*. Figure 5(a) indicates the absorption associated with a weak probe field whereas the present traces give the response when the strength of the probe field is increased to Rabi frequencies of Ω_{probe}=20, 100, and 150 kHz (lower trace to upper, respectively). Gain is increased by two orders of magnitude in comparison to that used in Fig. 4(a). The positions of the hyperfine resonances are indicated. (b) Direct measurements of the driven hyperfine transition using strong probe fields with Rabi frequencies as indicated. The positions of the subharmonic resonances are indicated.

Experimental measurements of subharmonic resonances are shown in Figs. 9(a) and 9(b). The one-photon case is shown in Fig. 9(b). Subharmonic resonances in this experimental system have been reported previously to our knowledge [14] and absorptive and emissive features are seen at displacements of $\pm\Omega_{hypX}$, $\pm\frac{1}{2}\Omega_{hypX}$, and $\pm\frac{1}{3}\Omega_{hypX}$ for probe fields with Rabi frequencies of Ω_{probe}=30 kHz; the features become clearer when the probe field is increased to Ω_{probe} =100 kHz. Equivalent resonances can be detected in the two-photon probe spectrum as shown in Fig. 9(a). Both the coupling and probe fields are involved. Simply increasing the strength of the coupling field leads to a broadening of the EIT features, and this is not appropriate as it will lead to a loss of the sharp features. Increasing the strength of the probe field saturates the absorption in the normal way and the signal strength is reduced. Although weak, a clear spectrum can still be detected when the signal is amplified. It can be seen that when the probe field has a Rabi frequency of 100 kHz, features at subharmonic frequencies are discernible. It can be concluded that there is again an equivalent observation of one- and two-photon probe fields. It is interesting to compare the processes involved in the two cases. In the conventional subharmonic resonance spectrum the first, second, and third features correspond to one-, three-, and five-photon transitions between dressed states. In this probe technique the first, second, and third resonances will correspond to two-, four-, and six-photon transitions between the driven two-level dressed states.

IX. CONCLUSION

The work in this paper presents an experimental investigation of an EIT perturbed by single and bichromatic driving fields. Various experimental investigations of this situation are compared with approximate density matrix calculations and dressed-state models. For most aspect of the spectra there is agreement between experiment and prediction and we conclude that the phenomena are being correctly interpreted. However, the area where there is poor agreement is in the prediction of the linewidths. The parameters have been obtained from independent measurements, and a calculation for a three-level system with no free parameters does give plausible agreement for the linewidth of the conventional EIT. The disagreement arises when driving the transition between the two lower levels. Calculation anticipates that EIT will be split and the split EIT features will be marginally broadened whereas the features are observed to be narrowed. The source of the disagreement is attributed to not including the effects of the inhomogeneous broadening of the lower transition. It is known that driving an inhomogeneous broadened two-level system causes a narrowing and the narrowing in the present situation is observed by direct measurement. It is found that there is a one-to-one comparison between the narrowing in the spectrum measured directly and that obtained in the EIT spectrum. This clearly indicates that the poor agreement is attributable to not allowing for the inhomogeneous nature of the width of the hyperfine transition. More elaborate calculations will be required to include these narrowing effects.

The principal motivation for the work has been to obtain a fundamental understanding of the behavior of an EIT with additional electromagnetic fields and this has been largely achieved with account given of the change to an EIT by single and bichromatic fields. The results have implications for the potential applications of EIT. A perturbing field can be used to open more than one EIT window and by controlling the strength and frequency of the perturbing field we can continuously vary the position of the transparencies, enabling EIT frequency tuning. The narrowing effects caused by the driving fields offer an even more exiting application as inhomogeneous broadening in hyperfine transitions in solid state system can often be significant and prohibit the observation of narrow transparencies. Introducing an additional driving field to narrow the EIT may make observation and application of EIT in such cases a more viable situation. Although the equivalent experiments at optical frequencies

will be more difficult, the present work has value in assessing the usefulness of the various perturbation schemes for controlling and modifying EIT features.

ACKNOWLEDGMENTS

This work was supported in part by the Australian Research Council and by DARPA through Texas Engineering Experimental Station. The authors are also appreciative of the use of a crystal from Professor S. Rand, University of Michigan.

APPENDIX

In this appendix we outline procedure for solving the density equation of motion given by Eqs. (1). The steady solution of Eqs. (1) can be written in terms of Fourier expansion as

$$W_{21} = \sum W_{21}(n)e^{-in\delta t},$$

$$W_{31} = \sum W_{31}(n)e^{-in\delta t},$$

$$\rho_{31} = \sum \rho_{31}(n)e^{-in\delta t},$$

$$\rho_{21} = \sum \rho_{21}(n)e^{-in\delta t},$$

$$\rho_{32} = \sum \rho_{32}(n)e^{-in\delta t}. \tag{A1}$$

Substituting Eqs. (A1) into Eqs. (1), we obtain a set of equations for the Fourier coefficients,

$$\begin{aligned}(2\gamma - in\delta)W_{21}(n) &= -i\chi_{probe}[\rho_{31}(n+1) - \rho_{13}(-n+1)] \\ &\quad + i\chi_{coup}[\rho_{32}(n) - \rho_{23}(-n)] \\ &\quad - 2i\chi_{hypX}[\rho_{21}(n) - \rho_{12}(-n)],\end{aligned}$$

$$\begin{aligned}(\gamma_3 - in\delta)W_{31}(n) &= -\frac{\gamma_3}{2}\delta_{n,0} - \left(\gamma - \frac{\gamma_3}{2}\right)W_{21}(n) \\ &\quad - 2i\chi_{probe}[\rho_{31}(n+1) - \rho_{13}(-n+1)] \\ &\quad - i\chi_{coup}[\rho_{32}(n) - \rho_{23}(-n)] \\ &\quad - i\chi_{hypX}[\rho_{21}(n) - \rho_{12}(-n)],\end{aligned}$$

$$\begin{aligned}(-d_{31} - in\delta)\rho_{31}(n) &= -i\chi_{probe}W_{31}(n-1) + i\chi_{coup}\rho_{21}(n) \\ &\quad - i\chi_{hypX}\rho_{32}(n),\end{aligned}$$

$$\begin{aligned}(-d_{21} - in\delta)\rho_{21}(n) &= -i\chi_{hypX}W_{21}(n) - i\chi_{probe}\rho_{23}(-n+1) \\ &\quad + i\chi_{coup}\rho_{31}(n),\end{aligned}$$

$$\begin{aligned}(-d_{32} - in\delta)\rho_{32}(n) &= i\chi_{probe}\rho_{12}(-n+1) \\ &\quad - i\chi_{coup}[W_{31}(n) - W_{21}(n)] \\ &\quad - i\chi_{hypX}\rho_{31}(n).\end{aligned} \tag{A2}$$

The perturbation approach is used to solve the above equations to first order of the weak probe field. To zero order of χ_{probe} the equations can be written as

$$\begin{aligned}(2\gamma - in\delta)W_{21}^{(0)}(n) &= i\chi_{coup}[\rho_{32}^{(0)}(n) - \rho_{23}^{(0)}(-n)] \\ &\quad - 2i\chi_{hypX}[\rho_{21}^{(0)}(n) - \rho_{12}^{(0)}(-n)],\end{aligned}$$

$$\begin{aligned}(\gamma_3 - in\delta)W_{31}^{(0)}(n) &= -\frac{\gamma_3}{2}\delta_{n,0} - \left(\gamma - \frac{\gamma_3}{2}\right)W_{21}^{(0)}(n) \\ &\quad - i\chi_{coup}[\rho_{32}^{(0)}(n) - \rho_{23}^{(0)}(-n)] \\ &\quad - i\chi_{hypX}[\rho_{21}^{(0)}(n) - \rho_{12}^{(0)}(-n)],\end{aligned}$$

$$(-d_{31} - in\delta)\rho_{31}^{(0)}(n) = +i\chi_{coup}\rho_{21}^{(0)}(n) - i\chi_{hypX}\rho_{32}^{(0)}(n),$$

$$(-d_{21} - in\delta)\rho_{21}^{(0)}(n) = -i\chi_{hypX}W_{21}^{(0)}(n) + i\chi_{coup}\rho_{31}^{(0)}(n),$$

$$\begin{aligned}(-d_{32} - in\delta)\rho_{32}^{(0)}(n) &= -i\chi_{coup}[W_{31}^{(0)}(n) - W_{21}^{(0)}(n)] \\ &\quad - i\chi_{hypX}\rho_{31}^{(0)}(n),\end{aligned} \tag{A3}$$

and to first order of χ_{probe} the equations can be written as

$$\begin{aligned}(2\gamma - in\delta)W_{21}^{(1)}(n) &= -i\chi_{probe}[\rho_{31}^{(0)}(n+1) - \rho_{13}^{(0)}(-n+1)] \\ &\quad + i\chi_{coup}[\rho_{32}^{(1)}(n) - \rho_{23}^{(1)}(-n)] \\ &\quad - 2i\chi_{hypX}[\rho_{21}^{(1)}(n) - \rho_{12}^{(1)}(-n)],\end{aligned}$$

$$\begin{aligned}(\gamma_3 - in\delta)W_{31}^{(1)}(n) &= -\left(\gamma - \frac{\gamma_3}{2}\right)W_{21}^{(1)}(n) - 2i\chi_{probe}[\rho_{31}^{(0)}(n+1) \\ &\quad - \rho_{13}^{(0)}(-n+1)] - i\chi_{coup}[\rho_{32}^{(1)}(n) - \rho_{23}^{(1)} \\ &\quad \times(-n)] - i\chi_{hypX}[\rho_{21}^{(1)}(n) - \rho_{12}^{(1)}(-n)],\end{aligned}$$

$$\begin{aligned}(-d_{31} - in\delta)\rho_{31}^{(1)}(n) &= -i\chi_{probe}W_{31}^{(0)}(n-1) + i\chi_{coup}\rho_{21}^{(1)}(n) \\ &\quad - i\chi_{hypX}\rho_{32}^{(1)}(n),\end{aligned}$$

$$\begin{aligned}(-d_{21} - in\delta)\rho_{21}^{(1)}(n) &= -i\chi_{hypX}W_{21}^{(1)}(n) - i\chi_{probe}\rho_{23}^{(0)}(-n+1) \\ &\quad + i\chi_{coup}\rho_{31}^{(1)}(n),\end{aligned}$$

$$\begin{aligned}(-d_{32} - in\delta)\rho_{32}^{(1)}(n) &= i\chi_{probe}\rho_{12}^{(0)}(-n+1) \\ &\quad - i\chi_{coup}[W_{31}^{(1)}(n) - W_{21}^{(1)}(n)] \\ &\quad - i\chi_{hypX}\rho_{31}^{(1)}(n).\end{aligned} \tag{A4}$$

It is straightforward, although tedious, to solve the above equations and the absorption response of the weak probe field is proportional to the imaginary part of the first-order solution of ρ_{31}, corresponding to $\rho_{31}^{(1)}$ in the notation adopted in this paper.

[1] E. Arimondo and G. Orriols, Lett. Nuovo Cimento Soc. Ital. Fis. **17**, 333 (1976).
[2] G. Alezetta, A. Gozzini, L. Moi, and G. Orriols, Nuovo Cimento Soc. Ital. Fis., B **36**, 5 (1976); H. M. Gray, R. M. Whitley, and C. R. Stroud, Jr., Opt. Lett. **3**, 218 (1978).
[3] G. Orriols, Nuovo Cimento Soc. Ital. Fis., B **53**, 1 (1979).
[4] S. E. Harris, Phys. Rev. Lett. **62**, 1033 (1989); M. O. Scully, S.-Y. Zhu, and A. Gavrielides, *ibid.* **62**, 2813 (1989); O. Kocharovskaya, Phys. Rep. **219**, 175 (1992); P. Mandel, Contemp. Phys. **34**, 235 (1993); A. S. Zibrov, M. D. Lukin, D. E. Nikonov, L. Hollberg, M. O. Scully, V. L. Velichansky, and H. G. Robinson, Phys. Rev. Lett. **75**, 1499 (1995); J. Mompart and R. Corbalan, J. Opt. B: Quantum Semiclassical Opt. **2**, R7 (2000).
[5] S. E. Harris, J. E. Field, and A. Imamoglu, Phys. Rev. Lett. **64**, 1107 (1990); M. O. Scully, *ibid.* **67**, 1855 (1991); M. Xiao, Y. Q. Li, S. Z. Jin, and J. Gea-Banacloche, *ibid.* **74**, 666 (1995); A. S. Zibrov, M. D. Lukin, L. Hollberg, D. E. Nikonov, M. O. Scully, H. G. Robinson, and V. L. Velichansky, *ibid.* **76**, 3935 (1996).
[6] A. Kasapi, M. Jain, G. Y. Yin, and S. E. Harris, Phys. Rev. Lett. **74**, 2447 (1995); O. Schmidt, R. Wynands, Z. Hussein, and D. Meschede, Phys. Rev. A **53**, R27 (1996); L. V. Hau, S. E. Harris, Z. Dutton, and C. H. Behroozi, Nature (London) **397**, 594 (1999); M. M. Kash, V. A. Sautenkov, A. S. Zibrov, L. Hollberg, G. R. Welch, M. D. Lukin, Y. Rostovtsev, E. S. Fry, and M. O. Scully, Phys. Rev. Lett. **82**, 5229 (1999).
[7] M. D. Lukin, S. F. Yelin, and M. Fleischhauer, Phys. Rev. Lett. **84**, 4232 (2000); C. Liu, Z. Dutton, C. H. Behroozi, and L. V. Hau, Nature (London) **409**, 490 (2001); D. F. Phillips, A. Fleischhauer, A. Mair, R. L. Walsworth, and M. D. Lukin, Phys. Rev. Lett. **86**, 783 (2001); O. Kocharovskaya, Y. Rostovtsev, and M. O. Scully, *ibid.* **86**, 628 (2001).
[8] M. H. Dunn, in *Laser Sources and Applications*, edited by A. Miller and D. M. Finlayson (Institute of Physics Publishing, Bristol, 1995), pp. 411–417; E. Arimondo, Prog. Opt. **35**, 257 (1996); J. P. Marangos, J. Mod. Opt. **45**, 471 (1998); Z. Ficek, Adv. Chem. Phys. **119**, 79 (2001); Y. Rostovtsev, I. Protsenko, H. Lee, and A. Javan, J. Mod. Opt. **49**, 2501 (2002).
[9] E. A. Wilson, N. B. Manson, and C. Wei, Phys. Rev. A **67**, 023812 (2003).
[10] S. R. de Echaniz, A. D. Greentree, A. V. Durrant, D. M. Segal, J. P. Marangos, and J. A. Vaccaro, Phys. Rev. A **64**, 013812 (2001); C. Y. Ye, A. S. Zibrov, and Yu. V. Rostovtsev, J. Mod. Opt. **49**, 391 (2002); C. Y. Ye, A. S. Zibrov, Yu. V. Rostovtsev, and M. O. Scully, Phys. Rev. A **65**, 043805 (2002).
[11] C. Wei and N. B. Manson, J. Opt. B: Quantum Semiclassical Opt. **1**, 464 (1999).
[12] C. Wei and N. B. Manson, Phys. Rev. A **60**, 2540 (1999).
[13] N. B. Manson, P. T. H. Fisk, and X.-F. He, Appl. Magn. Reson. **3**, 999 (1992); Changjiang Wei and Neil B. Manson, Phys. Rev. A **49**, 4751 (1994).
[14] N. B. Manson, C. Wei, and J. P. D. Martin, Phys. Rev. Lett. **76**, 3943 (1996).
[15] E. A. Wilson, N. B. Manson, and C. Wei, following paper, Phys. Rev. A **72**, 063814 (2005).
[16] G. Floquet, Ann. Sci. Ec. Normale Super. **12**, 47 (1883).
[17] S. J. Buckle, S. M. Barnett, P. L. Knight, M. A. Lauder, and D. T. Pegg, Opt. Acta **33**, 1129 (1986); D. Kosachiov, B. Matisov, and Yu. Rozhdestvensky, Opt. Commun. **85**, 209 (1991); H. Fearn, C. Keitel, M. O. Scully, and S.-Y. Zhu, *ibid.* **87**, 323 (1992).
[18] C. Cohen-Tannoudji and S. Reynaud, J. Phys. B **10**, 345 (1977); C. Cohen-Tannoudji, J. Dupont-Roc, and G. Grynberg, *Atom-Photon Interactions: Basic Processes and Applications* (Wiley, New York, 1992).
[19] A. D. Greentree, C. Wei, S. A. Holmstrom, J. P. D. Martin, N. B. Manson, K. R. Catchpole, and C. Savage, J. Opt. B: Quantum Semiclassical Opt. **1**, 240 (1999).
[20] B. R. Mollow, Phys. Rev. **188**, 1969 (1969).
[21] B. R. Mollow, Phys. Rev. A **5**, 2217 (1972); F. Y. Wu, R. E. Grove, and S. Ezekiel, Phys. Rev. Lett. **35**, 1426 (1975); F. Y. Wu, S. Ezekiel, M. Ducloy, and B. R. Mollow, *ibid.* **38**, 1077 (1977).
[22] P. Bucci, M. Martinelli, and S. Santucci, J. Chem. Phys. **53**, 4524 (1970); G. S. Agarwal and N. Nayak, J. Opt. Soc. Am. B **1**, 164 (1984); K. Koch, B. J. Oliver, S. Chakmakjian, and C. R. Stroud, Jr., *ibid.* **6**, 58 (1989); Y. Zhu, Q. Wu, S. Morin, and T. W. Mossberg, Phys. Rev. Lett. **65**, 1200 (1990); S. Papademetriou, S. Chakmakjian, and C. R. Stroud, J. Opt. Soc. Am. B **9**, 1182 (1992).
[23] S. H. Autler and C. H. Townes, Phys. Rev. **100**, 703 (1955).